Aberrant Collagen Composition of the Trabecular Meshwork Results in Reduced Aqueous Humor Drainage and Elevated IOP in MMP-9 Null Mice

Lies De Groef,[1,2] Lien Andries,[1] Anuja Siwakoti,[3] Emiel Geeraerts,[1] Ilse Bollaerts,[1] Lut Noterdaeme,[1] Isabelle Etienne,[4] Anna-Pia Papageorgiou,[5,6] Ingeborg Stalmans,[2] Johan Billen,[7] Judith A. West-Mays,[3] and Lieve Moons[1]

[1]Laboratory of Neural Circuit Development and Regeneration, Animal Physiology and Neurobiology Section, Department of Biology, KU Leuven, Leuven, Belgium
[2]Laboratory of Ophthalmology, Department of Neurosciences, KU Leuven, Leuven, Belgium
[3]Department of Pathology and Molecular Medicine, McMaster University Health Science Centre, Hamilton, Ontario, Canada
[4]ThromboGenics NV, Heverlee, Belgium
[5]Centre for Molecular and Vascular Biology (CMVB), Department of Cardiovascular Sciences, KU Leuven, Leuven, Belgium
[6]Cardiovascular Research Institute Maastricht (CARIM), Maastricht, The Netherlands
[7]Laboratory of Socioecology and Social Evolution, Ecology, Evolution and Biodiversity Conservation Section, Department of Biology, KU Leuven, Leuven, Belgium

Correspondence: Lieve Moons, Research Group Neural Circuit Development and Regeneration, Animal Physiology and Neurobiology Section, Department of Biology, KU Leuven, Naamsestraat 61 Box 2464, B-3000 Leuven, Belgium; lieve.moons@kuleuven.be.

Submitted: April 12, 2016
Accepted: September 16, 2016

Citation: De Groef L, Andries L, Siwakoti A, et al. Aberrant collagen composition of the trabecular meshwork results in reduced aqueous humor drainage and elevated IOP in MMP-9 null mice. *Invest Ophthalmol Vis Sci*. 2016;57:5984–5995. DOI: 10.1167/iovs.16-19734

Purpose. Homeostatic turnover of the trabecular meshwork extracellular matrix (ECM) is essential to regulate aqueous humor outflow and to maintain intraocular pressure homeostasis. In this study, we evaluated aqueous humor turnover, intraocular pressure, and trabecular meshwork organization in MMP-9 null mice.

Methods. Intraocular pressure and aqueous humor turnover were measured in MMP-9 null versus wild-type mice. Morphology of the anterior segment of the eye, with special attention to the structural organization of the trabecular meshwork, was investigated by means of optical coherence tomography, light microscopy, and transmission electron microscopy. Furthermore, using quantitative real-time polymerase chain reaction and immunostainings, we evaluated the ECM composition of the trabecular meshwork. Finally, the integrity and function of the retina and optic nerve were assessed, via optical coherence tomography, histologic techniques, and optomotor testing.

Results. MMP-9 null mice displayed early-onset ocular hypertension and reduced aqueous humor turnover. While transmission electron microscopic analysis did not reveal any abnormalities in the cellular organization of the trabecular meshwork, detailed investigation of collagen expression indicated that there is an aberrant trabecular meshwork ECM composition in MMP-9 null mice. Notably, at the age of 13 months, no glaucomatous neurodegeneration was seen in MMP-9 null mice.

Conclusions. Our observations corroborate MMP-9 as an important remodeler of the collagenous composition of the trabecular meshwork and provide evidence for a causal link between MMP-9 deficiency, trabecular meshwork ultrastructure, and ocular hypertension.

Keywords: intraocular pressure, matrix metalloproteinase-9, aqueous humor dynamics, collagen

Glaucoma is one of the most common blinding diseases, affecting more than 60 million people worldwide.[1,2] Although the disease presents as a neurodegenerative disorder affecting retinal ganglion cell (RGC) axons in the optic nerve and their somata in the retina, the elicitors of this optic neuropathy are often located outside the neuroretina. Ocular hypertension, resulting from disturbances in aqueous humor turnover, is considered to be the major risk factor for the development of glaucoma.

The intraocular pressure (IOP) is defined by the rate of aqueous humor production by the ciliary body on the one hand, and the aqueous humor outflow resistance via the iridocorneal tissues (i.e., trabecular meshwork and Schlemm's canal) and the uveoscleral pathway, on the other hand. The trabecular meshwork is largely responsible for the generation of the outflow resistance via homeostatic turnover of its extracellular matrix (ECM).[3,4] This complex equilibrium of ECM biosynthesis versus proteolysis is actualized by, among others, members of the matrix metalloproteinase (MMP) family. Matrix metalloproteinase-1, -2, -3, -9, -12, and -14, as well as their endogenous inhibitors TIMP-1 to -4, are constitutively expressed by trabecular meshwork cells.[3,5–9] Their balanced, concerted activity results in cleavage of the intricate supermolecular organization of the trabecular ECM, thereby allowing

Investigative Ophthalmology & Visual Science

endocytosis and intracellular degradation of these cleavage products by the trabecular meshwork cells. In general, mechanical stretching of the trabecular meshwork due to IOP elevation, is believed to induce upregulated secretion of MMPs, while reducing TIMPs. This altered MMP/TIMP balance increases the trabecular ECM turnover rate, reduces the aqueous outflow resistance, and restores normal IOP.[10]

Matrix metalloproteinases are a well-conserved family of metzincin proteases. Based on either their structural organization or their substrate preference, MMPs are categorized into smaller subfamilies that together can cleave virtually all components of the ECM.[11–13] Matrix metalloproteinase-9 (gelatinase B, 92-kDa type IV collagenase) belongs to the subfamily of the gelatinases. In general, MMP-9 is essential to reproduction, growth and development, inflammation and would healing, whereas it plays a detrimental role in many inflammatory, infectious, degenerative, and vascular diseases.[13–15] In the eye, only one publication[16] has described ocular hypertension in MMP-9 null mice. In addition, MMP-9 deficiency has been reported to protect against detachment-induced apoptosis of the RGCs in an ischemia–reperfusion injury model.[17] Other anomalies seen in MMP-9 null mice include bone-development defects, delayed healing of bone fractures, impaired vascular remodeling and reduced angiogenesis, and defective neuronal remyelination after nerve injury.[13,15]

In this study, we aimed to fully characterize the ocular phenotype of MMP-9 null mice, with emphasis on the potential dysregulation of IOP in these mice. Therefore, we performed a detailed characterization of IOP homeostasis and aqueous humor turnover, as well as a morphologic investigation of the anterior segment of the eye. Special attention was given to the structural organization of the trabecular meshwork, which was investigated both at the light microscopic level and by means of transmission electron microscopy. Furthermore, we evaluated the qualitative ECM composition of the trabecular meshwork, by means of quantitative real-time polymerase chain reaction (qRT-PCR) and immunostainings. Finally, the integrity of the retina and optic nerve was assessed to reveal whether MMP-9 null mice suffer from ocular hypertension-induced RGC degeneration.

Materials and Methods

Experimental Animals

All studies were conducted in compliance with the ARVO Statement for the Use of Animals in Ophthalmic and Vision Research, and were approved by the institutional ethical committees. Wild-type and MMP-9 null (MMP-9$^{-/-}$) mice in the C57Bl6/N genetic background were obtained from the university breeding colony and genotyped to confirm homozygosity.[18] Knockdown of MMP-9 was verified by using gelatin zymography on tissue lysates of the anterior chamber angle region (data not shown). Animals were kept under a 12/12-hour light–dark cycle and had ad libitum access to food and water.

Intraocular Pressure Measurement and Pachymetry

A rebound tonometer (Tono-Lab; iCare, Helsinki, Finland) was used to measure the IOP in anesthetized animals, according to the manufacturer's instructions. Intraocular pressure measurements were taken between 3 and 5 minutes after induction of anesthesia with avertin (intraperitoneal [i.p.] 15 mL/kg; Sigma-Aldrich Corp., St. Louis, MO, USA). Following IOP measurement, central corneal thickness (CCT) was assessed by using an ultrasound pachymeter (Corneao Plus; Sonogage, Cleveland, OH, USA), as previously described.[19]

Noninvasive Measurement of Aqueous Humor Turnover

Aqueous humor turnover was measured noninvasively by monitoring the rate of fluorescence decay from the aqueous humor after topical instillation of fluorescein.[20] Fluorescence images were captured in 10-minute intervals for 1 hour, with a stereomicroscope (Zeiss, Oberkochen, Germany). For each image, the average pixel intensity in the green channel was calculated by using Fiji software.[21] The first fluorescence image was used as the peak fluorescence (100%, $t = 0$) for normalizing all subsequent measurements. Experiments were performed under general anesthesia with ketamine (i.p. 75 mg/kg, Nimatek; Eurovet Animal Health, Bladel, the Netherlands) and medetomidine (i.p. 1 mg/kg, Domitor; Janssen Pharmaceutica, Beerse, Belgium).

Spectral-Domain Optical Coherence Tomography (SD-OCT)

Anterior segment morphology and thickness of the retinal layers were evaluated in anesthetized mice, with an SD-OCT system (Envisu R2210; Bioptigen, Morrisville, NC, USA).[22] Spectral-domain OCT was performed by using 100 consecutive B-scan lines composed of 1000 A-scans, in a 3.0 × 3.0-mm (anterior segment) or 1.4 × 1.4-mm field (retina). Anterior chamber depth, CCT, total retinal thickness, and thickness of the ganglion cell complex were analyzed by using InVivoVue Diver 2.2 software (Bioptigen).

Histologic Stainings

For histologic analysis of the retina, cornea, anterior segment, and axon integrity, semithin 1-μm cross-sections were made. Eyes were fixed overnight in cold 2% glutaraldehyde (in 150 mM saccharose, 50 mM sodium cacodylate [pH 7.3]), followed by fixation in 2% osmium tetroxide (in 50 mM sodium cacodylate [pH 7.3]) for 1 hour. After dehydration in a graded acetone series, tissues were embedded in Araldite. Eye sections were stained with 0.1% methylene blue and 0.1% thionine (in 115 mM $Na_2HPO_4.2H_2O$); optic nerve sections were stained with 1% toluidine blue (in 500 mM sodium borohydride).[23] Images were taken with a light microscope (Zeiss). Axonal integrity was qualitatively evaluated by using the grading scale described by Jia et al. (five sections per mouse).[24,25] In addition, the radius of the optic nerve was measured (three sections per mouse) and axon density (number of axons/100 μm^2) was semiautomatically computed by using a validated sampling method (five frames of 7500 μm^2 per mouse), based on the Particle Counter plugin for Fiji software.[21,23]

For Picro Sirius Red staining of collagen, paraffin sections of the eye were stained for 1 hour with Direct Red 80 (0.1% in aqueous solution of picric acid; Sigma-Aldrich Corp.), followed by 2 minutes rinsing in 0.01N HCl. Images were taken with a polarized light microscope (Leica, Wetzlar, Germany). For analysis of Sirius Red stainings, the iridocorneal tissue was outlined and the average pixel intensity in the red and green channel was analyzed in this region of interest (five sections per mouse), using Fiji software.

A Verhoeff's Van Gieson staining on paraffin sections was used to visualize elastin fibers. Briefly, sections were incubated for 20 minutes in Verhoeff's Elastica (hematoxylin 5%, $FeCl_3$ 10%, lugol, in a 120:48:48 ratio), followed by 2 minutes in

Investigative Ophthalmology & Visual Science

ferric chloride 2%, 2 minutes in ethanol 95%, and 6 minutes in Van Gieson (acid fuchsin 1%, saturated picric acid, in a 1:45 ratio). Images were taken with a light microscope (Zeiss).

Quantification of RGC Survival via Brn3a Immunostaining

Brna3 immunostaining was performed on retinal flat-mounts.[26,27] Briefly, whole mount retinas were frozen for 15 minutes at −80°C, and the primary antibody goat anti-Brn3a (1:750, C-20; Santa Cruz Biotechnology, Dallas, TX, USA) was applied overnight. The next day, retinas were incubated with a secondary antibody conjugated to Alexa fluorophore-488 (1:500; Life Technologies, Carlsbad, CA, USA) for 2 hours. Mosaic z-stack images of the entire retina were taken with a multiphoton microscope (Olympus, Tokyo, Japan). Retinal ganglion cell density (number of $Brn3a^+$ RGCs/mm^2) and heat maps representing a pseudocolor representation of RGC density were automatically computed from whole mount retinas, by using Fiji software and a recently described semiautomated counting macro.[28]

Immunostainings for Collagens and Fibronectin

Immunostainings for fibronectin and collagen I and IV were performed on 10-μm paraffin-embedded sections. Briefly, antigen retrieval was performed by heating the sections in citrate buffer for 20 minutes at 95°C. Sections were incubated for 20 minutes in 0.3% hydrogen peroxide (only for collagen stainings), followed by a 1-hour blocking step with 20% preimmune serum and overnight incubation with the primary antibody (rabbit anti-collagen I, 1:500, ab34710, Abcam, Cambridge, UK; rabbit anti-collagen IV, 1:400, 2150-1470, AbD Serotec, Düsseldorf, Germany; rabbit anti-fibronectin, 1:100, F3648, Sigma-Aldrich Corp.). For the collagen stainings, the secondary biotin-conjugated antibody (1:300; Dako, Glostrup, Denmark) was applied for 45 minutes, and fluorescein isothiocyanate tyramide signal amplification was performed according to the manufacturer's instructions (Perkin-Elmer, Waltham, MA, USA). For the fibronectin staining, an Alexa fluorophore–conjugated secondary antibody (Life Technologies) was applied for 1 hour. Images were taken with a confocal microscope (Olympus).

Transmission Electron Microscopy

Ultrathin (70 nm) transverse sections of Araldite-embedded optic nerves were placed on 50 mesh copper grids, and double stained with 4% uranyl acetate (in 50% ethanol) for 15 minutes and 3% lead citrate for 4 minutes. Images were taken with an EM900 transmission electron microscope (Zeiss). Trabecular meshwork organization was analyzed on images of the entire trabecular meshwork by using Fiji software. Thickness of individual trabecular beams and the total trabecular meshwork were measured at 30-μm increments along the length of the trabecular meshwork. The intertrabecular space was marked by background color filling. This area was then divided by the length of the trabecular meshwork along which it was analyzed, thus yielding a relative measure for intertrabecular space.

Quantitative RT-PCR

Transcript levels of ECM molecules (collagen I, collagen IV, elastin, and fibronectin), TIMPs (TIMP-1, -2, -3, and -4) and compensatory MMPs (MMP-2, -3, and -13) were analyzed at mRNA level with a qRT-PCR. *Top1*, *Actb*, and *Gapdh* were selected from a list of five potential housekeeping genes by using the geNorm reference gene analysis (Biogazelle, Ghent, Belgium).[29] Upon euthanization, the tissues of the iridocorneal angle were quickly dissected and snapfrozen, followed by RNA isolation with TRI Reagent (Sigma-Aldrich Corp.) and the NucleoSpin RNA II kit (Macherey-Nagel, Düren, Germany). First-strand cDNA was synthetized from 250 ng RNA, using Superscript III Reverse Transcriptase (Life Technologies). Next, qRT-PCR was performed by using either SYBR Green Mastermix (Thermo Fischer Scientific, Waltham, MA, USA) and 250 nM of both primers (for ECM molecules and TIMPs), or Maxima Probe/ROX qPCR Master Mix (Life Technologies) and 125 nM TaqMan PrimeTime qPCR Assay (for MMPs). Primers, probes (Integrated DNA Technologies, Coralville, IA, USA), and annealing temperatures are listed in Table 1. All samples were run in triplicate with the StepOne Plus system (Applied Biosystems, Foster City, CA, USA), and a no-template control was added as negative control. Relative expression was determined by using qBase software (based on the ΔΔCT method) (Biogazelle)[30] and normalized against the geometric mean of the housekeeping genes.

Statistics

For all data, normal distribution and parallel equal variance between groups were tested. Intraocular pressure measurements and pachymetry data were analyzed with a 2-way ANOVA followed by Sidak's multiple comparisons test. Aqueous humor turnover data were analyzed by using a 2-way repeated-measures ANOVA followed by Sidak's multiple comparisons test. Exponential decay constants were calculated by least-squares regression analysis for exponential decay ($[\%\ \text{Intensity}] = 100.e^{-k.\text{time}}$). All other data were analyzed by using a Student's *t*-test. A probability level of <0.05 was accepted as statistically significant ($^*P < 0.05$, $^{**}P < 0.01$, $^{***}P < 0.001$, $^{****}P < 0.0001$). All data are presented as mean ± SEM. Statistical analyses were performed with GraphPad Prism 6 (GraphPad Software, La Jolla, CA, USA).

Results

Intraocular Pressure Homeostasis and Aqueous Humor Dynamics

Measurements of the IOP confirmed that in each age group studied, MMP-9 null mice had a significantly higher IOP than age-matched wild-type mice ($P < 0.0001$). A 27%, 37%, 50%, and 40% increase was observed at the age of 2 to 3, 3 to 4, 6 to 8 and 9 to 12 months (Fig. 1a). Of note, ultrasound pachymetry excluded a difference in CCT between wild-type and MMP-9 null mice (Fig. 1b). Furthermore, fluorophotometric measurements of aqueous humor dynamics at the age of 13 months revealed that aqueous humor turnover was significantly delayed in MMP-9 null animals, as shown by a lower exponential decay constant (0.006 min^{-1}, $R^2 = 0.82$) in comparison to wild-type mice (0.011 min^{-1}, $R^2 = 0.98$) ($P < 0.05$). Multiple comparisons analysis indeed revealed significantly higher fluorescence intensities in MMP-9 null than in wild-type mice at 20 ($P < 0.01$), 30 ($P < 0.05$), 40 ($P < 0.05$), and 50 minutes ($P < 0.05$) post application of fluorescein (Figs. 1c, 1d).

Anterior Segment Morphology

Next, potential malformations at the level of the iridocorneal angle were evaluated in wild-type and MMP-9 null mice at the age of 13 months. Spectral-domain OCT imaging of the anterior segment of the eye confirmed that neither the wild-type nor

Investigative Ophthalmology & Visual Science

Table 1. Sequences of qRT-PCR Primers, Probes, and Annealing Temperatures

Probe/Primer	Sequence	Annealing Temperature
SYBR Green assays		
Musm_*Eln*_F	5′-TGGTGACATGATCCCTCTCTCTT-3′	62.5°C
Musm_*Eln*_R	5′-CCAGGGTGTCCCAGATGTG-3′	
Musm_*Fn1*_F	5′-ATCATTTCATGCCAACCAGTT-3′	59.5°C
Musm_*Fn1*_R	5′-TCGCACTGGTAGAAGTTCCA-3′	
Musm_*Col1a1*_F	5′-CGATGGATTCCCGTTCGAGT-3′	60.5°C
Musm_*Col1a1*_R	5′-CGATCTCGTTGGATCCCTGG-3′	
Musm_*Col4a3*_F	5′-TGTGGATGCACGGTGTGTT-3′	62.5°C
Musm_ *Col4a3*_R	5′-GTTCTCTTCACGGTGTGCTTGA-3′	
Musm_*Timp1*_F	5′-CCAGAACCGCAGTGAAGAGT-3′	57.0°C
Musm_*Timp1*_R	5′-GTACGCCAGGGAACCAAGAA-3′	
Musm_*Timp2*_F	5′-CAGCCTCTCCCGTCTTTTGT-3′	60.5°C
Musm_*Timp2*_R	5′-GTGGCTAGAAACCCCAGCAT-3′	
Musm_*Timp3*_F	5′-GGACAGACTTGAGGTGAGGC-3′	62.5°C
Musm_*Timp3*_R	5′-AGACCTCAAAAGCCGACTGG-3′	
Musm_*Timp4*_F	5′-TTTGACCATCACCACCTGCTGT-3′	64.5°C
Musm_ *Timp4*_R	5′-ACTTCAGCCAAACAGCCCACTC-3′	
Musm_*Actb*_F	5′-CGAGCGTGGCTACAGCTTCA-3′	60.5°C
Musm_*Actb*_R	5′-GAGCCACCGATCCACACAGA-3′	
Musm_*Gapdh*_F	5′-TTCACCACCATGGAGAAGGC-3′	62.5°C
Musm_*Gapdh*_R	5′-GGCATGGACTGTGGTCATGA-3′	
Musm_*Top1*_F	5′-TGCCAGAGAGTGTCAAGTTT-3′	59.5°C
Musm_*Top1*_R	5′-GCTCATCTGTGTAAAGTCGC-3′	
Musm_*Gusb*_F	5′-GTATGAACGGGAAGCAATCC-3′	59.0°C
Musm_*Gusb*_R	5′-AATCCCATTCACCCACACAA-3′	
Musm_*Ywhaz*_F	5′-ACCCATCTTCCTTTACAACTCA-3′	64.5°C
Musm_*Ywhaz*_R	5′-CATCCTGCTGTCCATTGCTTA-3′	
TaqMan assays		
Mmp2 (Mm.PT.58.9606100)	5′- /56-FAM/CACCCTTGA/ZEN/AGAAGTAGCTATGACCACC/3IABkFQ/ -3′	60.0°C
Musm_*Mmp2*_F	5′-AACTTCACGCTCTTGAGACTT-3′	
Musm_*Mmp2*_R	5′-GAATGCCATCCCTGATAACCT-3′	
Mmp3 (Mm.PT. 58.9719290)	5′- /56-FAM/TGGTTGCTG/ZEN/CTCATGAACTTGGC/3IABkFQ/ -3′	60.0°C
Musm_*Mmp3*_1_F	5′-GATGAACGATGGACAGAGGATG-3′	
Musm_*Mmp3*_1_R	5′-TGTGGAGGACTTGTAGACTGG-3′	
Mmp13 (Mm.PT.58.42286812)	5′- /56-FAM/AGGGCTGGG/ZEN/TCACACTTCTCTG/3IABkFQ/ -3′	60.0°C
Musm_*Mmp13*_F	5′-AGACTGGTAATGGCATCAAGG-3′	
Musm_*Mmp13*_R	5′-GCCATTTCATGCTTCCTGATG-3′	

the MMP-9 null mice had a closed iridocorneal angle, and also anterior chamber depth did not differ (Figs. 2a, 2b). An additional light microscopy histologic survey on transverse sections of the eye revealed a normal ciliary body, well-defined trabecular meshwork, and a patent Schlemm's canal in all mice (Fig. 2c).

Trabecular Meshwork Ultrastructure and ECM Composition

Together, the above findings indicate that the underlying cause of the observed ocular hypertension in MMP-9 null mice might be due to abnormalities on an ultrastructural level, for example, the (sub)cellular organization and/or ECM composition of the iridocorneal angle. Nevertheless, transmission electron microscopy revealed giant vacuoles in the inner wall endothelium of Schlemm's canal, indicating a pressure gradient and aqueous humor outflow, in both wild-type and MMP-9 null mice (Fig. 3a). Furthermore, morphometric analysis of the thickness of individual trabecular beams and the total thickness of the trabecular meshwork, as well as the intertrabecular space, did not reveal any difference in the laminar organization of the trabecular meshwork in wild-type and MMP-9 null mice (Fig. 3b). As such, the overall organization of the trabecular meshwork does not seem to be affected by MMP-9 deficiency.

In contrast, qRT-PCR analysis of collagen transcript levels unveiled that collagen I (*Col1a1*; $P = 0.064$) and collagen IV (*Col4a3*; $P = 0.067$) expression tended to be lower in MMP-9 null mice (Figs. 4a, 4d). Immunostainings on transverse sections of the anterior segment of the eyes confirmed a prominent decrease in collagen I expression in the ECM in MMP-9 null mice (Figs. 4b, 4c). In contrast, collagen IV differences in immunolabeling were less pronounced and confined to basal laminae (Figs. 4e, 4f). Furthermore, analysis of Sirius Red staining on adjacent sections showed, first, a slight decrease (~20%) in total collagen staining in the trabecular meshwork of MMP-9 null mice ($P < 0.05$), and second, an altered ratio of mature versus immature collagen. Indeed, an increased accumulation of mature collagen ($P < 0.005$) was seen in the trabecular meshwork of MMP-9 null mice, while immature collagen was significantly decreased ($P < 0.05$) (Figs. 5a–c).

Expression analysis of elastin and fibronectin, using qRT-PCR and (immuno)histologic stainings, did not reveal any significant differences in expression between wild-type and MMP-9 null mice (Supplementary Fig. S1).

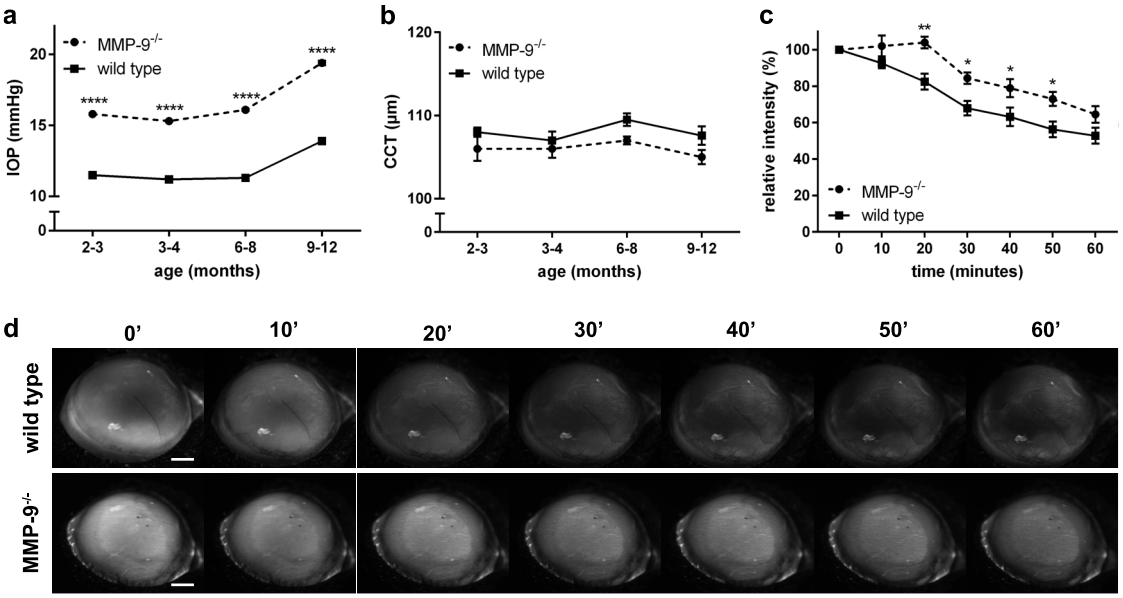

Figure 1. MMP-9 null mice exhibit elevated IOP owing to reduced aqueous humor drainage. (**a**) Longitudinal follow-up of IOP in wild-type and MMP-9 null mice revealed that IOP elevation already manifests from the age of 2 months and persists at all ages measured thereafter, in MMP-9 null mice ($n \geq 8$, 2-way ANOVA, $P < 0.0001$). (**b**) Ultrasound pachymetry revealed no difference in CCT between wild-type and MMP-9 null mice ($n \geq 8$, 2-way ANOVA). (**c**) Fluorophotometric measurements revealed that aqueous humor turnover is delayed in MMP-9 null animals (age 13 months) ($n = 5$, 2-way repeated-measures ANOVA, $P < 0.05$). (**d**) Representative series of fluorescence images captured from wild-type and MMP-9 null mice at 10-minute intervals after application of fluorescein. *Scale bar*: 1 mm.

Implications of MMP-9 Deficiency on Retinal Integrity

Given the IOP elevation observed in MMP-9 null animals, we next investigated whether these mice exhibit a glaucoma-like phenotype, that is, whether they exhibit RGC degeneration and/or optic neuropathy. Analysis of total retinal thickness and thickness of the ganglion cell complex (GCC, i.e., the sum of the nerve fiber layer, RGC layer, and inner plexiform layer) on SD-OCT images of the retina revealed no difference between wild-type and MMP-9 null mice at the age of 13 months (Figs. 6a, 6b). Furthermore, qualitative assessment of retinal morphology on transverse sections of the retina did not show any abnormalities (Fig. 6e). In line with these observations, evaluation of RGC density on retinal whole mounts did not disclose any differences between wild-type and MMP-9 null mice, in either young mice (3 months) or old mice (13 months) (Figs. 6c, 6d). Finally, little to no signs of glaucomatous optic neuropathy were seen on toluidine blue–stained semithin sections of the optic nerve (Fig. 6h). Qualitative one-to-five

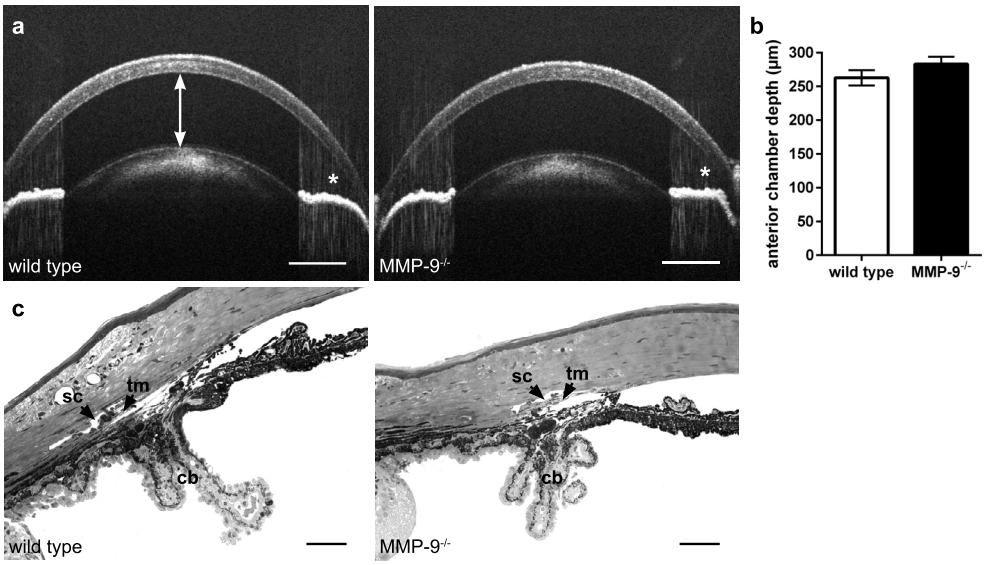

Figure 2. MMP-9 null mice exhibit normal overall anterior segment morphology. (**a**) Spectral- domain OCT imaging of the anterior segment of the eye showed an open iridocorneal angle (*) in all mice under study. (**b**) In addition, morphometric analysis of the anterior chamber depth (*arrow*) indicated that there is no difference between wild-type and MMP-9 null mice (age 13 months) ($n \geq 13$, Student's *t*-test). *Scale bar*: 500 µm. (**c**) Postmortem histologic analysis of the anterior segment revealed no overt changes in the ciliary body (cb), trabecular meshwork (tm), and Schlemm's canal (sc) of MMP-9 null mice ($n = 5$) as compared to age-matched wild-type mice ($n = 7$). *Scale bar*: 50 µm.

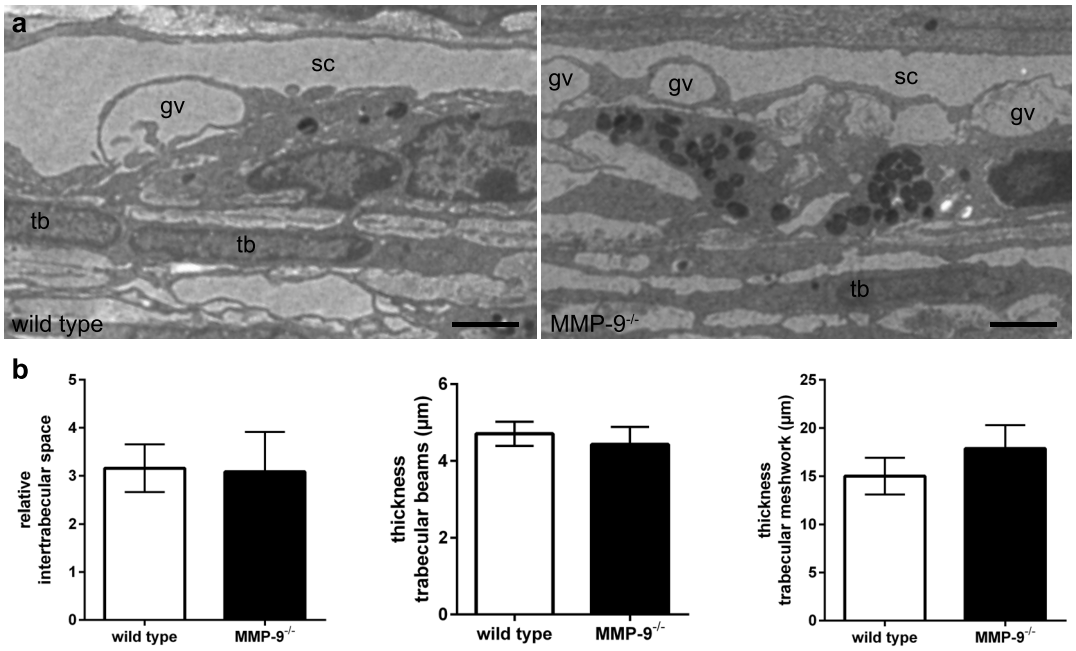

Figure 3. MMP-9 null mice exhibit normal laminar organization of the trabecular meshwork. (**a**) Representative transmission electron microscopy images of the trabecular meshwork of wild-type and MMP-9 null mice, illustrating normal laminar organization of the trabecular meshwork and the presence of giant vacuoles (gv) in the inner wall endothelium of Schlemm's canal (sc). *Scale bar*: 2 µm. (**b**) Morphometric analysis did not detect any difference in the thickness of the trabecular beams (tb), the trabecular meshwork, or the intertrabecular space ($n \geq 3$, Student's *t*-test).

grading of axonal integrity resulted in equal scores for wild-type and MMP-9 null mice. Moreover, the optic nerve radius (143 ± 9 µm versus 162 ± 4 µm, respectively) and axonal density (39 ± 5 axons/100 µm^2 versus 44 ± 13 axons/100 µm^2, respectively) did not differ between wild-type and MMP-9 null mice (Figs. 6f, 6g).

Expression Profiling of TIMPs and Selected MMPs in MMP-9 Null Mice

Enzymatic redundancy and compensation have been suggested as underlying causes for the—often surprisingly—subtle phenotypes of MMP-deficient mice.[13] Following a literature search and analysis of MMP substrate repertoires, we selected MMP-2, MMP-3, and MMP-13 as the most plausible candidates for compensation of MMP-9 enzymatic activities in MMP-9 null mice. We performed a qRT-PCR expression analysis of these MMPs in iridocorneal angle tissue extracts and found that for all three MMPs, mRNA expression levels tended to be lower in MMP-9 null mice ($P < 0.05$ for *Mmp13*) (Table 2). These results thus preclude compensatory transcription of these MMPs. Second, we also evaluated coregulation of TIMP expression. Whereas mRNA levels of *Timp1*, *Timp2*, and *Timp3* were equal in wild-type and MMP-9 null mice, a significant elevation (~80% increase; $P < 0.05$) was seen for *Timp4* in the anterior chamber angle tissue of MMP-9 null mice. Thus, no coincidental decrease in TIMP levels, which could compensate for decreased MMP(–9) activity, was found.

Discussion

MMP-9 Plays an Essential Role in Maintaining the Ultrastructural Organization of the Trabecular Meshwork

In accordance with earlier reports,[16] the present results demonstrated that MMP-9 null mice exhibit early-onset ocular hypertension. In vivo measurements of aqueous humor dynamics indicated that this ocular hypertension is related to a decreased aqueous humor turnover, which could either be the result of increased aqueous humor production or increased outflow resistance. Given the aberrant collagen composition of the iridocorneal angle that we observed in this study in MMP-9 null mice and other correlations between MMP-9, trabecular meshwork ECM remodeling, and regulation of aqueous humor outflow resistance,[10] we postulate that the underlying cause of the ocular hypertension observed in MMP-9 null mice is an increased aqueous humor outflow resistance generated in the trabecular meshwork. This rationale is further supported by our SD-OCT and light microscopy analyses, which did not unveil any abnormalities of the iridocorneal angle, ciliary body, trabecular meshwork, or Schlemm's canal in MMP-9 null mice. The underlying cause for the increased outflow resistance observed in MMP-9 null mice should thus reside in the ultrastructural architecture/composition of the trabecular meshwork. Indeed, while transmission electron microscopy revealed no difference in the organization of the trabecular beams and intertrabecular space, combined data from qRT-PCR and immunostainings for collagen I and detailed analysis of Sirius Red stainings indicated a differential ECM composition and disturbed ECM turnover in MMP-9 null mice. From these findings, we hypothesize that MMP-9 deficiency results in reduced degradation of mature collagen fibers in MMP-9 null mice, which in turn negatively affects de novo synthesis of (immature) collagen (Fig. 5c). Indeed, the resultant accumulation of mature collagen fibers in the iridocorneal angle of MMP-9 null mice is reflected in the more intense labeling of mature collagen in the Sirius Red stainings, while the negative feedback regulation of collagen transcription can be seen in the reduced levels of *Col1a1* and *Col4a3* mRNA and the attenuated amount of immature collagen after analysis of Sirius Red stainings. Notably, although the collagen I antibody used in this study was produced by using the full collagen polypeptide as an immunogen, and should therefore bind to both

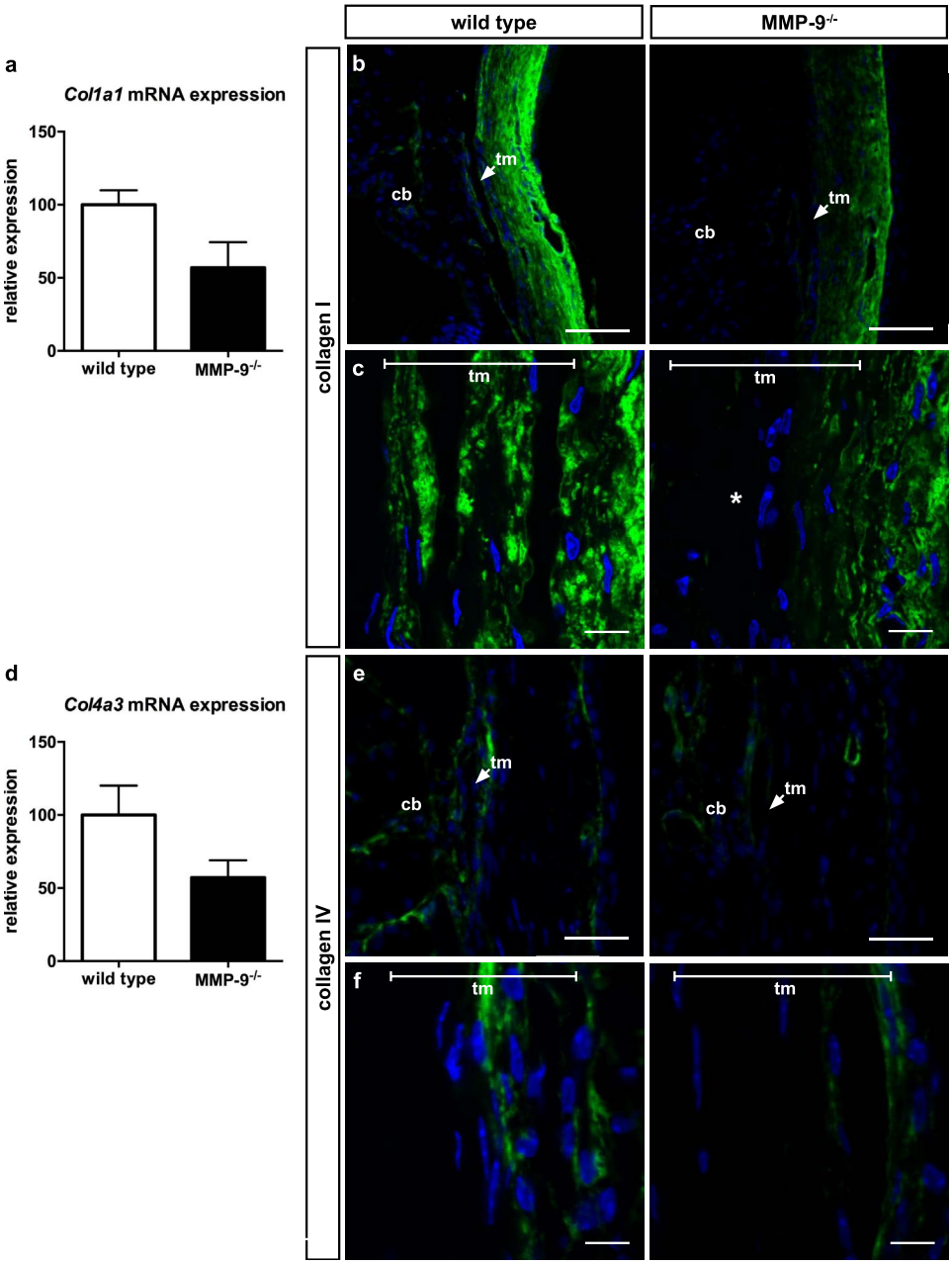

Figure 4. Collagen synthesis is affected in MMP-9 null mice. (**a**) qPCR analysis of *Col1a1* mRNA expression reveals a (nonsignificant) reduction of approximately 50% in collagen I synthesis in MMP-9 null mice in comparison to wild-type mice ($n = 6$, Student's *t*-test). (**b**) Overview picture of a collagen I immunostaining of the anterior chamber angle region, showing reduced collagen I expression in the trabecular meshwork and the sclera of MMP-9 null mice. *Scale bar*: 50 μm. (**c**) High-magnification image of collagen I staining in the trabecular meshwork, revealing nearly complete absence of collagen I staining in the trabecular beams of MMP-9 null mice (*). *Scale bar*: 10 μm. (**d**) qPCR analysis of *Col4a3* mRNA expression reveals a (nonsignificant) reduction of approximately 50% in collagen IV synthesis in MMP-9 null mice in comparison to wild-type mice ($n = 6$, Student's *t*-test). (**e**) Overview picture of collagen IV immunostaining of the anterior chamber angle region reveals that immunostaining intensity is slightly reduced in the trabecular meshwork of MMP-9 null mice. *Scale bar*: 50 μm. (**f**) High-magnification image of collagen IV staining in the trabecular meshwork confirms reduced collagen IV immunolabeling. *Scale bar*: 10 μm.

monomeric and fibrillar forms of collagen I, our results suggest that an increase in mature collagen I (fibrils) coincides with reduced immunoreactivity. This leads us to believe that the reduced immunoreactivity might be the result of cryptic epitopes exclusively buried within the structure of the fibrillar form, as has been described before for other polypeptides that form mono-/oligomeric and fibrillar assemblies.[31]

Several lines of evidence point out that the trabecular meshwork ECM is indeed the source of aqueous humor outflow resistance, and that MMP-9 is a potent modulator of the trabecular meshwork architecture. Ultrastructural examinations of the trabecular meshwork of POAG patients reveal a shift in ECM composition as well as decreased MMP-9 activity, and a reciprocal interplay between both.[32–34] Furthermore, overexpression of the matricellular protein SPARC in human anterior segment explant cultures results in elevated IOP and qualitative changes in the ECM of the trabecular meshwork (i.e., elevated collagen I, IV, and VI; laminin; and fibronectin

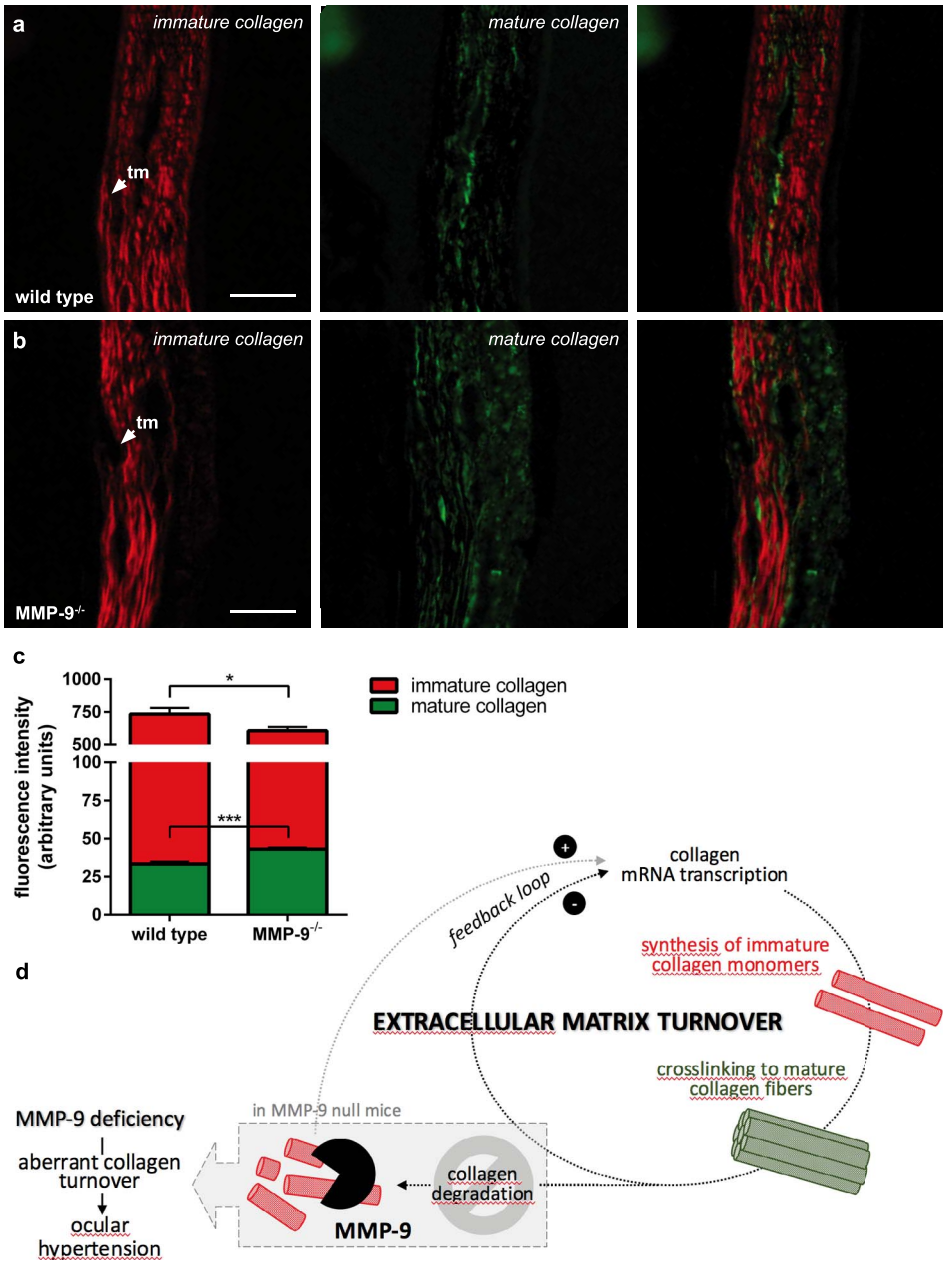

Figure 5. Sirius Red staining on sections of the iridocorneal angle reveals a disturbed collagen turnover in MMP-9 null mice. (**a**, **b**) Sirius Red staining reveals immature collagen (i.e., non–cross-linked collagen monomers) in *red*, and mature collagen (i.e., cross-linked bundles of collagen fibers) in *green*. *Scale bar*: 50 μm. (**c**) MMP-9 null mice display an altered ratio of immature versus mature collagen, compared to wild-type animals: more mature collagen and less immature collagen is seen ($n = 6$; Student's *t*-test). (**d**) These observations could be explained by the hypothesis schematically depicted here. Owing to the lack of MMP-9 proteolytic activity in MMP-9 null mice, degradation of mature collagen is impeded. As a result of feedback signaling mechanisms, this results in an increased suppression and/or decreased activation of collagen gene transcription, which leads to a lowered synthesis of immature collagen monomers.

levels) that could be linked to a shift in MMP/TIMP balance and a selective decrease in MMP-9 activity.[33,35] This evidence for an important role for MMP-9 in IOP homeostasis has been corroborated by in vitro experiments using perfused human anterior segment organ cultures, to which addition of recombinant MMP-9 results in a reversible increase in outflow facility.[36] Notably, increased concentrations of TIMP-4 have been found in the aqueous humor of POAG patients,[37,38] supposedly adding to the imbalance in the MMP/TIMP molar ratio. Despite a proven correlation with ocular hypertension, it remains unresolved whether these changes are a cause or consequence of the disease and whether TIMP levels increase in response to altered MMP secretion or vice versa. Notably, several MMP-independent activities have been proposed for TIMPs, including TIMP-4, such as regulation of cell growth, differentiation, migration, and apoptosis.[39] In the context of the trabecular meshwork, these actions could directly inhibit cell contractibility and phagocytosis, and/or lead to the loss of cellularity that has been observed within the POAG trabecular meshwork, thereby affecting aqueous humor drainage.[37,38] In conclusion, although TIMP-4 is a known inhibitor of MMP-9,[40] it remains elusive to what extent it is involved in the aberrant collagen turnover that we observed in the trabecular meshwork of MMP-9 null mice. Continued research is required to

Investigative Ophthalmology & Visual Science

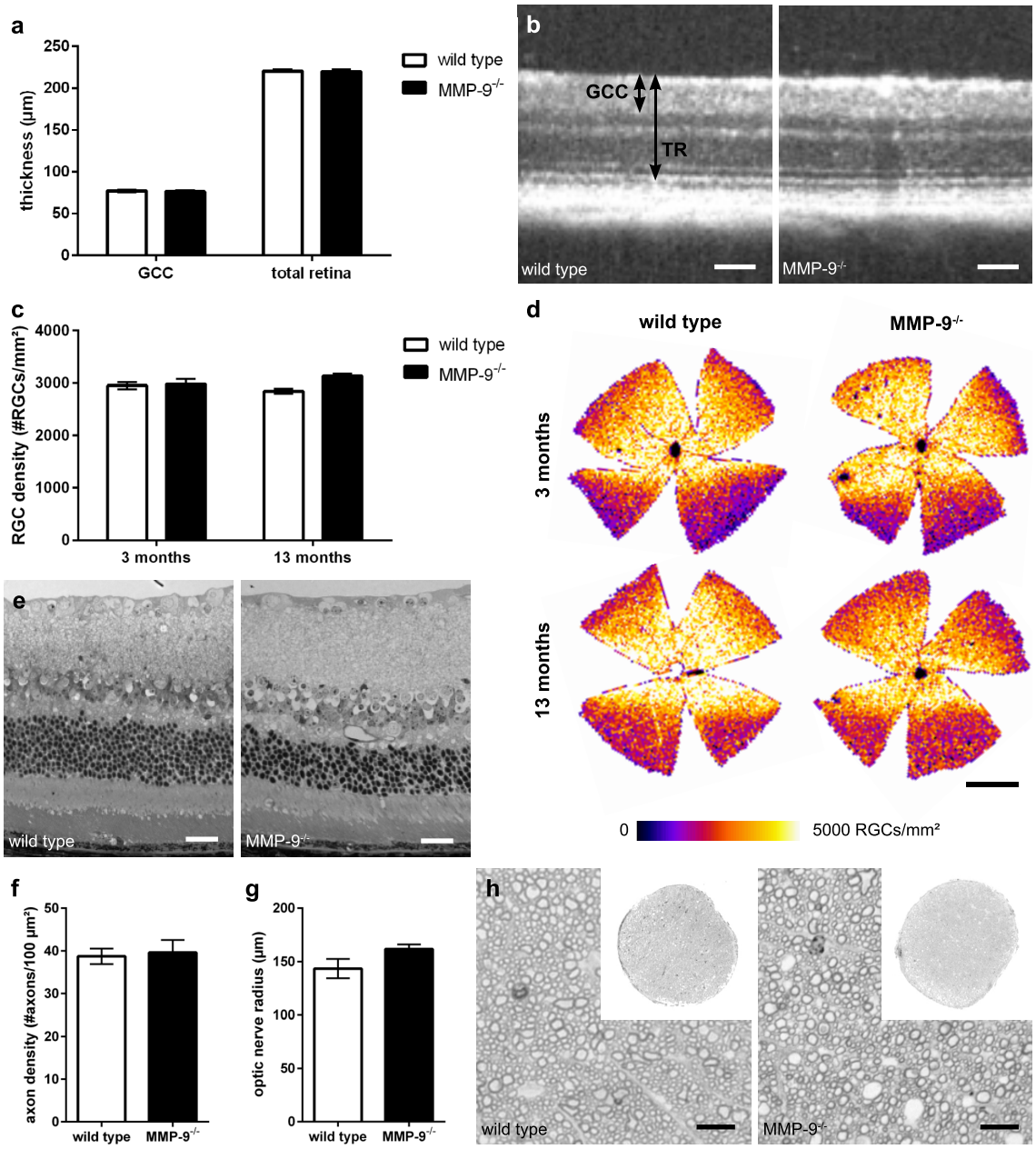

Figure 6. MMP-9 null mice exhibit no signs of retinal atrophy or optic neuropathy. (**a**, **b**) Morphometric analysis of the thickness of the total retina (TR, *arrow*) and the thickness of the GCC (*arrow*) on SD-OCT images of the retina revealed no significant differences between 13-month-old wild-type ($n = 15$) and MMP-9 null mice ($n = 13$) (Student's *t*-test). *Scale bar*: 50 µm. (**c**, **d**) Retinal ganglion cell density, quantified as the number of Brn3a$^+$ cells per mm^2 retina and represented via pseudocolor density mapping here, was similar in wild-type and MMP-9 null mice and did not change between the age of 3 and 13 months (Student's *t*-test). *Scale bar*: 1 mm. (**e**) Postmortem histologic analysis of the retina revealed no overt changes in cytoarchitecture of 13-month-old wild-type mice ($n = 7$) versus age-matched MMP-9 null mice ($n = 5$). *Scale bar*: 20 µm. (**f**) Measurements of the optic nerve diameter revealed no difference between 13-month-old wild-type ($n = 7$) and MMP-9 null mice ($n = 6$) (Student's *t*-test). (**g**) Quantification of axonal density in the optic nerves of 13-month-old wild-type ($n = 7$) and MMP-9 null mice ($n = 6$) revealed no effect of MMP-9 deficiency on axonal integrity (Student's *t*-test). (**h**) Toluidine blue staining on optic nerve cross-sections of wild-type and MMP-9 null mice. *Scale bar*: 10 µm.

uncover the biological effects of the increased TIMP-4 expression, with respect to its potential effects on both ECM composition and on the cellular organization of the trabecular meshwork. The exact role of collagens in the regulation of outflow resistance remains unclear, yet evidence for a crucial effect on IOP homeostasis is emerging. Whereas type I, III, and IV collagen fibers are constituents of the basement membrane–like material in the intercellular space of the trabecular meshwork and confer tensile strength to the tissue, collagen types III and VI are found in the sheets of the elastic fibers that allow expansion and recoil of the trabecular meshwork in response to IOP fluctuations.[41,42] Notably, POAG and aging are associated with structural changes in the trabecular meshwork, including accumulation of both type VI collagen and elastic fiber sheet material.[43–48] Furthermore, disorganization of the collagenous ECM appears to be a common theme in several transgenic mouse lines displaying ocular hypertension and glaucomatous neurodegeneration. In *Cyp1b1*$^{-/-}$ mice, irregular collagen distribution in the trabecular meshwork and elevated IOP are seen, resembling the abnormalities in the trabecular

Table 2. Messenger RNA Expression Levels of TIMPs and Selected MMPs in the Iridocorneal Angle of Wild-Type Versus MMP-9 Null Mice

Gene of Interest	Wild Type	MMP-9$^{-/-}$	*t*-test
Timp1	0.952 ± 0.189	1.177 ± 0.074	n.s.
Timp2	0.996 ± 0.105	1.065 ± 0.107	n.s.
Timp3	1.365 ± 0.283	0.967 ± 0.182	n.s.
Timp4	0.717 ± 0.111	1.305 ± 0.173	$P < 0.05$
Mmp2	1.399 ± 0.248	0.837 ± 0.120	n.s.
Mmp3	1.214 ± 0.320	1.090 ± 0.141	n.s.
Mmp13	1.280 ± 0.126	0.848 ± 0.119	$P < 0.05$

Summary of mRNA expression levels (mean ± SEM; $n = 6$; Student's *t*-test). n.s., not significant.

meshwork of human primary congenital glaucoma patients.[42,49] Trabecular meshwork collagen fibrils have also been found to be larger and more irregular in thrombospondin-1 and -2 null mice, which display decreased IOP.[50] Notably, thrombospondin-1, -2, and SPARC have been shown to modulate MMP levels.[51] Finally, the transgenic *Colla1*$^{r/r}$ mouse—with a targeted mutation in the *Colla1* gene, abolishing the consensus cleavage site for MMP-1, -2, and potentially other MMPs—displays gradual IOP elevation and axonal degeneration.[52,53] This has been attributed to an age-dependent accumulation of collagen I in the outflow pathways, due to inhibition of fibrillar collagen turnover, and a reduced outflow facility is found in these mice.[52,54] Taken together, disruption of collagen fibers in the trabecular meshwork may decrease tissue elasticity, alter the shape and cytoskeletal organization of trabecular meshwork cells, and affect expansion–recoil of the trabecular spaces, leading to a compromised aqueous humor outflow and disturbed IOP homeostasis. Of note, a coinvolvement of trabecular and uveoscleral outflow pathways seems plausible, as the observed imbalance of collagen turnover in both these tissues will impede aqueous humor outflow via either route.[54]

The Role of MMP-9 in the Retina Seems to Be Limited to a Detrimental Function

As elevated IOP is the major risk factor for glaucoma, we hypothesized that the MMP-9 null mice would be predisposed to develop glaucomatous optic neuropathy. We therefore analyzed total retinal thickness to check for overall retinal atrophy, GCC thickness and RGC density to assess RGC degeneration, and axon density in the optic nerve to evaluate axonal integrity. Taken together, none of these analyses revealed any signs of glaucomatous neurodegeneration in the retina or optic nerve of MMP-9 null and wild-type mice. These results are in line with the surprisingly subtle phenotypes that have been described in many other MMP null mouse lines, and that have been attributed to enzymatic redundancy, enzymatic compensation, and adaptive development.[13]

Nevertheless, several genetic mouse models for glaucoma have shown that IOP elevations of the magnitude observed in this study are sufficient to induce optic neuropathy, although these IOP elevations all manifested at later ages. This is the case in, for example, DBA/2J, *Colla1*$^{r/r}$, and Tyr437His mice.[53,55–57] Why is RGC degeneration or axonal damage absent in MMP-9 null mice despite a clear early-onset IOP elevation? As we excluded both coincidental decreases in TIMP levels and enzymatic compensation for deleted MMP-9 activity by MMP-2, MMP-3, and MMP-13, the most likely explanation may lie either in MMP redundancy or in MMP-9 functioning in the retina. Increased MMP-9 activity in the RGC layer has indeed been reported in diverse glaucoma models and plays a key role in the promotion of RGC death, by inducing degradation of laminin and subsequent detachment-induced apoptosis of RGCs.[58–60] Remarkably, MMP-9 null mice subjected to an optic nerve ligation injury model are protected from RGC death,[17] suggesting that MMP-9 null mice are protected from glaucomatous neurodegeneration. An alternative explanation might be related to the presence of collagens in the peripapillary ECM, which may, according to preliminary findings (Supplementary Fig. S2), be affected in the MMP-9 null mice. According to the mechanical stress hypothesis, ocular hypertension-induced distortions of the ECM surrounding the RGC axon bundles are at the basis of glaucomatous damage. The qualitative composition of the ECM may thus have a major impact on its stress resistance and, therefore, on the susceptibility of RGC (axons) to glaucomatous neurodegeneration.[61,62]

Therapeutic Implications

Several studies in POAG patients have linked decreased MMP-9 activity in the trabecular meshwork to the development of ocular hypertension.[33,34] The present results endorse a causal role for MMP-9 and put forward this ECM-remodeling protease as a potential target for novel IOP-lowering therapies. Noteworthy, ocular hypertension has already been successfully reversed via viral vector–mediated delivery of MMP-1 in the trabecular meshwork of sheep with steroid-induced glaucoma.[63,64] A similar, viral vector–mediated approach to overexpress MMP-9 in the trabecular meshwork could be persued. On the other hand, given its detrimental role in RGC degeneration, direct manipulation of MMP-9 activity in the eye might be a dangerous approach for the treatment of glaucoma. Alternatively, the present data could be a starting point to identify downstream molecules of MMP-9 regulation and novel targets for baroprotective therapies.

Acknowledgments

The authors thank Véronique Brouwers, An Vandoren, Sofie Beckers, Sven Zels, Alexander Ball, and Amadeo Rodriguez for excellent technical assistance and fruitful discussions; Rita Van Ginderdeuren for help with the interpretation of trabecular meshwork morphology; and Valerie Van Heukelom and Bart Jonckx for SD-OCT training.

Supported by the KU Leuven Research Council (BOF-OT/10/033 [LM]); the Hercules Foundation (AKUL-09-038, AKUL1309 [LM]); the Research Foundation Flanders (G.05311.10 [LM]); fellowship IB); the Flemish government agency for Innovation by Science and Technology (fellowship LDG, EG); the American Health Assistance Foundation National Glaucoma Research Award (now BrightFocus) (JAW-M); the Ontario Graduate Scholarship (AS); and the National Institutes of Health (NEI, EY025789 [JAW-M]). The authors alone are responsible for the content and writing of the paper.

Disclosure: **L. De Groef**, None; **L. Andries**, None; **A. Siwakoti**, None; **E. Geeraerts**, None; **I. Bollaerts**, None; **L. Noterdaeme**, None; **I. Etienne**, Thrombogenics NV (E); **A.-P. Papageorgiou**, None; **I. Stalmans**, None; **J. Billen**, None; **J.A. West-Mays**, None; **L. Moons**, None

References

1. Quigley HA. Glaucoma. *The Lancet*. 2011;377:1367–1377.
2. Quigley HA, Broman AT. The number of people with glaucoma worldwide in 2010 and 2020. *Br J Ophthalmol*. 2006;90:262–267.
3. Bradley JM, Kelley MJ, Rose A, Acott TS. Signaling pathways used in trabecular matrix metalloproteinase response to

mechanical stretch. *Invest Ophthalmol Vis Sci*. 2003;44:5174–5181.

4. Bradley JM, Kelley MJ, Zhu X, Anderssohn AM, Alexander JP, Acott TS. Effects of mechanical stretching on trabecular matrix metalloproteinases. *Invest Ophthalmol Vis Sci*. 2001;42:1505–1513.
5. Kelley MJ, Rose AY, Song K, et al. Synergism of TNF and IL-1 in the induction of matrix metalloproteinase-3 in trabecular meshwork. *Invest Ophthalmol Vis Sci*. 2007;48:2634–2643.
6. Oh DJ, Martin JL, Williams AJ, Russell P, Birk DE, Rhee DJ. Effect of latanoprost on the expression of matrix metalloproteinases and their tissue inhibitors in human trabecular meshwork cells. *Invest Ophthalmol Vis Sci*. 2006;47:3887–3895.
7. Pang IH, Hellberg PE, Fleenor DL, Jacobson N, Clark AF. Expression of matrix metalloproteinases and their inhibitors in human trabecular meshwork cells. *Invest Ophthalmol Vis Sci*. 2003;44:3485–3493.
8. Alexander JP, Samples JR, Van Buskirk EM, Acott TS. Expression of matrix metalloproteinases and inhibitor by human trabecular meshwork. *Invest Ophthalmol Vis Sci*. 1991;32:172–180.
9. WuDunn D. The effect of mechanical strain on matrix metalloproteinase production by bovine trabecular meshwork cells. *Curr Eye Res*. 2001;22:394–397.
10. De Groef L, Van Hove I, Dekeyster E, Stalmans I, Moons L. MMPs in the trabecular meshwork: promising targets for future glaucoma therapies? *Invest Ophthalmol Vis Sci*. 2013;54:7756–7763.
11. Rosenberg GA. Matrix metalloproteinases and their multiple roles in neurodegenerative diseases. *Lancet Neurol*. 2009;8:205–216.
12. Ethell IM, Ethell DW. Matrix metalloproteinases in brain development and remodeling: synaptic functions and targets. *J Neurosci Res*. 2007;85:2813–2823.
13. Page-McCaw A, Ewald AJ, Werb Z. Matrix metalloproteinases and the regulation of tissue remodelling. *Nat Rev Mol Cell Biol*. 2007;8:221–233.
14. Verslegers M, Lemmens K, Van Hove I, Moons L. Matrix metalloproteinase-2 and –9 as promising benefactors in development plasticity and repair of the nervous system. *Prog Neurobiol*. 2013;105:60–78.
15. Van den Steen PE, Dubois B, Nelissen I, Rudd PM, Dwek RA, Opdenakker G. Biochemistry and molecular biology of gelatinase B or matrix metalloproteinase-9 (MMP-9). *Crit Rev Biochem Mol Biol*. 2002;37:375–536.
16. Robertson JV, Siwakoti A, West-Mays AS. Altered expression of transforming growth factor beta 1 and matrix metalloproteinase-9 results in elevated intraocular pressure in mice. *Mol Vis*. 2013;19:684–695.
17. Chintala SK, Zhang X, Austin JS, Fini ME. Deficiency in matrix metalloproteinase gelatinase B (MMP-9) protects against retinal ganglion cell death after optic nerve ligation. *J Biol Chem*. 2002;277:47461–47468.
18. Vu TH, Shipley JM, Bergers G, et al. MMP-9/gelatinase B is a key regulator of growth plate angiogenesis and apoptosis of hypertrophic chondrocytes. *Cell*. 1998;93:411–422.
19. Lively GD, Jiang B, Hedberg-Buenz A, et al. Genetic dependence of central corneal thickness among inbred strains of mice. *Invest Ophthalmol Vis Sci*. 2010;51:160–171.
20. Avila MY, Mitchell CH, Stone RA, Civan MM. Noninvasive assessment of aqueous humor turnover in the mouse eye. *Invest Ophthalmol Vis Sci*. 2003;44:722–727.
21. Schindelin J, Arganda-Carreras I, Frise E, et al. Fiji: an open-source platform for biological-image analysis. *Nat Methods*. 2012;9:676–682.
22. Buys ES, Ko YC, Alt C, et al. Soluble guanylate cyclase alpha1-deficient mice: a novel murine model for primary open angle glaucoma. *PLoS One*. 2013;8:e60156.
23. Marina N, Bull ND, Martin KR. A semiautomated targeted sampling method to assess optic nerve axonal loss in a rat model of glaucoma. *Nat Protoc*. 2010;5:1642–1651.
24. Morrison JC, Johnson EC, Cepurna W, Jia L. Understanding mechanisms of pressure-induced optic nerve damage. *Prog Retin Eye Res*. 2005;24:217–240.
25. Jia L, Cepurna WO, Johnson EC, Morrison JC. Patterns of intraocular pressure elevation after aqueous humor outflow obstruction in rats. *Invest Ophthalmol Vis Sci*. 2000;41:1380–1385.
26. Galindo-Romero C, Aviles-Trigueros M, Jimenez-Lopez M, et al. Axotomy-induced retinal ganglion cell death in adult mice: quantitative and topographic time course analyses. *Exp Eye Res*. 2011;92:377–387.
27. Nadal-Nicolas FM, Jimenez-Lopez M, Sobrado-Calvo P, et al. Brn3a as a marker of retinal ganglion cells: qualitative and quantitative time course studies in naive and optic nerve-injured retinas. *Invest Ophthalmol Vis Sci*. 2009;50:3860–3868.
28. Geeraerts E, Dekeyster E, Gaublomme D, Salinas-Navarro M, De Groef L, Moons L. A freely available semi-automated method for quantifying retinal ganglion cells in entire retinal flatmounts. *Exp Eye Res*. 2015;147:105–113.
29. Vandesompele J, De Preter K, Pattyn F, et al. Accurate normalization of real-time quantitative RT-PCR data by geometric averaging of multiple internal control genes. *Genome Biol*. 2002;3:RESEARCH0034.
30. Hellemans J, Mortier G, De Paepe A, Speleman F, Vandesompele J. qBase relative quantification framework and software for management and automated analysis of real-time quantitative PCR data. *Genome Biol*. 2007;8:R19.
31. Brännström K, Lindhagen-Persson M, Gharibyan AL, et al. A generic method for design of oligomer-specific antibodies. *PLoS One*. 2014;9:e90857.
32. Knepper PA, Goossens W, Hvizd M, Palmberg PF. Glycosaminoglycans of the human trabecular meshwork in primary open-angle glaucoma. *Invest Ophthalmol Vis Sci*. 1996;37:1360–1367.
33. Oh D-J, Kang MH, Ooi YH, Choi KR, Sage EH, Rhee DJ. Overexpression of SPARC in human trabecular meshwork increases intraocular pressure and alters extracellular matrix. *Invest Ophthalmol Vis Sci*. 2013;54:3309–3319.
34. Guo MS, Wu YY, Liang ZB. Hyaluronic acid increases MMP-2 and MMP-9 expressions in cultured trabecular meshwork cells from patients with primary open-angle glaucoma. *Mol Vis*. 2012;18:1175–1181.
35. Haddadin RI, Oh D-J, Kang MH, et al. SPARC-null mice exhibit lower intraocular pressures. *Invest Ophthalmol Vis Sci*. 2009;50:3771–3777.
36. Bradley JM, Vranka J, Colvis CM, et al. Effect of matrix metalloproteinases activity on outflow in perfused human organ culture. *Invest Ophthalmol Vis Sci*. 1998;39:2649–2658.
37. Briggs ELA, Toh TY, Eri R, Hewitt AW, Cook AL. TIMP1, TIMP2, and TIMP4 are increased in aqueous humor from primary open angle glaucoma patients. *Mol Vis*. 2015;21:1162–1172.
38. Fountoulakis N, Labiris G, Aristeidou A, et al. Tissue inhibitor of metalloproteinase 4 in aqueous humor of patients with primary open angle glaucoma pseudoexfoliation syndrome and pseudoexfoliative glaucoma and its role in proteolysis imbalance. *BMC Ophthalmol*. 2013;13:1–7.
39. Stetler-Stevenson WG. Tissue inhibitors of metalloproteinases in cell signaling: metalloproteinase-independent biological activities. *Sci Signal*. 2008;1:re6.
40. Baker AH, Edwards DR, Murphy G. Metalloproteinase inhibitors: biological actions and therapeutic opportunities. *J Cell Sci*. 2002;115:3719–3727.

Investigative Ophthalmology & Visual Science

41. Keller KE, Acott TS. The juxtacanalicular region of ocular trabecular meshwork: a tissue with a unique extracellular matrix and specialized function. *J Ocul Biol*. 2013;1:3.
42. Teixeira LB, Zhao Y, Dubielzig RR, Sorenson CM, Sheibani N. Ultrastructural abnormalities of the trabecular meshwork extracellular matrix in Cyp1b1-deficient mice. *Vet Pathol*. 2015;52:397–403.
43. Tektas OY, Lutjen-Drecoll E. Structural changes of the trabecular meshwork in different kinds of glaucoma. *Exp Eye Res*. 2009;88:769–775.
44. Lutjen-Drecoll E, Rittig M, Rauterberg J, Jander R, Mollenhauer J. Immunomicroscopical study of type VI collagen in the trabecular meshwork of normal and glaucomatous eyes. *Exp Eye Res*. 1989;48:139–147.
45. Lutjen-Drecoll E, Futa R, Rohen JW. Ultrahistochemical studies on tangential sections of the trabecular meshwork in normal and glaucomatous eyes. *Invest Ophthalmol Vis Sci*. 1981;21: 563–573.
46. Gabelt BT, Kaufman PL. Changes in aqueous humor dynamics with age and glaucoma. *Prog Retin Eye Res*. 2005;24:612–637.
47. Rohen JW, Lutjen-Drecoll E, Flugel C, Meyer M, Grierson I. Ultrastructure of the trabecular meshwork in untreated cases of primary open-angle glaucoma (POAG). *Exp Eye Res*. 1993; 56:683–692.
48. Gottanka J, Johnson DH, Martus P, Lutjen-Drecoll E. Severity of optic nerve damage in eyes with POAG is correlated with changes in the trabecular meshwork. *J Glaucoma*. 1997;6: 123–132.
49. Zhao Y, Wang S, Sorenson CM, et al. Cyp1b1 mediates periostin regulation of trabecular meshwork development by suppression of oxidative stress. *Mol Cell Biol*. 2013;33:4225–4240.
50. Haddadin RI, Oh D-J, Kang MH, et al. Thrombospondin-1 (TSP1)–null and TSP2-null mice exhibit lower intraocular pressures. *Invest Ophthalmol Vis Sci*. 2012;53:6708–6717.
51. Kyriakides TR, Bornstein P. Matricellular proteins as modulators of wound healing and the foreign body response. *Thromb Haemost*. 2003;90:986–992.
52. Aihara M, Lindsey JD, Weinreb RN. Ocular hypertension in mice with a targeted type I collagen mutation. *Invest Ophthalmol Vis Sci*. 2003;44:1581–1585.
53. Mabuchi F, Lindsey JD, Aihara M, Mackey MR, Weinreb RN. Optic nerve damage in mice with a targeted type I collagen mutation. *Invest Ophthalmol Vis Sci*. 2004;45:1841–1845.
54. Dai Y, Lindsey JD, Duong-Polk X, Nguyen D, Hofer A, Weinreb RN. Outflow facility in mice with a targeted type I collagen mutation. *Invest Ophthalmol Vis Sci*. 2009;50:5749–5753.
55. Libby RT, Anderson MG, Pang IH, et al. Inherited glaucoma in DBA/2J mice: pertinent disease features for studying the neurodegeneration. *Vis Neurosci*. 2005;22:637–648.
56. Zhou Y, Grinchuk O, Tomarev SI. Transgenic mice expressing the Tyr437His mutant of human myocilin protein develop glaucoma. *Invest Ophthalmol Vis Sci*. 2008;49:1932–1939.
57. Senatorov V, Malyukova I, Fariss R, et al. Expression of mutated mouse myocilin induces open-angle glaucoma in transgenic mice. *J Neurosci*. 2006;26:11903–11914.
58. Santos ARC, Corredor RG, Obeso BA, et al. Beta1 integrin-focal adhesion kinase (FAK) signaling modulates retinal ganglion cell (RGC) survival. *PLoS One* 2012;7:e48332.
59. Guo L, Moss SE, Alexander RA, Ali RR, Fitzke FW, Cordeiro MF. Retinal ganglion cell apoptosis in glaucoma is related to intraocular pressure and IOP-induced effects on extracellular matrix. *Invest Ophthalmol Vis Sci*. 2005;46:175–182.
60. Halfter W, Willem M, Mayer U. Basement membrane-dependent survival of retinal ganglion cells. *Invest Ophthalmol Vis Sci*. 2005;46:1000–1009.
61. Nguyen C, Cone FE, Nguyen TD, et al. Studies of scleral biomechanical behavior related to susceptibility for retinal ganglion cell loss in experimental mouse glaucoma. *Invest Ophthalmol Vis Sci*. 2013;54:1767–1780.
62. Burgoyne CF. A biomechanical paradigm for axonal insult within the optic nerve head. *Exp Eye Res*. 2011;93:120–132.
63. Gerometta R, Spiga MG, Borras T, Candia OA. Treatment of sheep steroid-induced ocular hypertension with a glucocorticoid-inducible MMP1 gene therapy virus. *Invest Ophthalmol Vis Sci*. 2010;51:3042–3048.
64. Spiga MG, Borras T. Development of a gene therapy virus with a glucocorticoid-inducible MMP1 for the treatment of steroid glaucoma. *Invest Ophthalmol Vis Sci*. 2010;51:3029–3041.

Investigative Ophthalmology & Visual Science